Science Journal of University of Zakho
DOI: https://doi.org/10.25271/sjuoz

Original Article

SYNTHESIS, SPECTROSCOPIC CHARACTERIZATION, AND COMPARATIVE ANTIBACTERIAL SCREENING OF CONDENSATION-DERIVED Cu (II) AND Zn(II) COMPLEXES

Falah M. Darweesh[1], Muzhda Q. Qader[1], Sewgil S. Anwer[2, 3] Lubna A. Abdulkarim[4], Thana Y. Yousif[5], and R. Ranjith Kumar [6, *]

1 Department of Public Health, Hawler Medical University, Kurdistan Region, Iraq.
2 Clinical Biochemistry Department, Hawler Medical University, Kurdistan Region, Iraq.
3 Nursing Department, Tishk International University, Erbil, Iraq.
4 Department of Environmental Sciences, Salahaddin University-Erbil, Kurdistan Region, Iraq.
5 Department of New and Renewable Energies, College of Science, University of Mosul, Mosul, Iraq.
6 Department of Botany, Madras Christian College (Autonomous) Affiliated to The University of Madras, Chennai, Tamil Nadu, India.

*Corresponding author, E-mail: ranjithkumar@mcc.edu.in (Tel: +91-9941466607)

Received: 30, Nov, 2025

Accepted: 24, Mar, 2026

Published: 12, Apr, 2026

ABSTRACT

Condensation-derived ligands and their transition metal complexes continue to attract interest due to their structural versatility and potential biological applications. In this study, the tetraaza ligand 2,5,7,10-tetraaza-1,6(1,3)-dibenzenacyclodecaphene-3,4,8,9-tetraone (TF) was synthesized via a microwave-assisted protocol and coordinated with Cu(II) and Zn(II) ions. The ligand and its complexes were characterized by elemental analysis, FTIR, UV–Vis spectroscopy, molar conductance, NMR spectroscopy (ligand), and magnetic measurements. Metal content analysis supports a 1:1 metal–ligand stoichiometry, and the complexes are tentatively formulated as [M(TF)] (M = Cu(II), Zn(II)). Spectroscopic data indicate predominant coordination through nitrogen donor atoms, while carbonyl groups remain non-coordinating. The Cu(II) complex exhibited paramagnetic behavior consistent with a configuration; whereas, the Zn(II) analogue was diamagnetic. Antibacterial activity evaluated against Staphylococcus aureus and Pseudomonas aeruginosa revealed enhanced activity for the Cu(II) complex compared to the Zn(II) complex and the free ligand. Although metal coordination significantly influenced antibacterial performance, definitive structural and mechanistic investigations are required to establish detailed structure–activity relationships.

KEYWORDS: Condensation-derived ligand, Copper(II) complex, Zinc(II) complex, Coordination chemistry, Antibacterial activity.

1. INTRODUCTION

The rapid escalation of antimicrobial resistance (AMR) represents one of the most pressing global challenges to contemporary healthcare systems (Salam *et al.*, 2023). Among the most clinically significant pathogens are *Staphylococcus aureus* and *Pseudomonas aeruginosa*, both recognized for their adaptability, biofilm-forming capacity, and propensity to develop resistance to multiple antibiotic classes (Almatroudi, 2025; Kollef *et al.*, 2021; Salam *et al.*, 2023). Several classes of antibiotics, such as β-lactams, aminoglycosides, quinolones, and polymyxins, have been widely used to treat infections caused by these organisms (Muteeb *et al.*, 2023). Transition metal complexes have emerged as promising alternatives due to their diverse coordination chemistry and ability to disrupt bacterial physiology through unique mechanisms (Claudel *et al.*, 2020). A range of coordination networks can be formed by these condensation based ligands and have strong chelation sites, modularity of design, and pharmacophores with good structural adaptability (Khan *et al.*, 2022). When coordinated with transition metals such as Cu(II) and Zn(II), these ligands may yield complexes with altered membrane permeability and biological activity, depending on the metal center (El-Lateef *et al.*, 2023; Riccardi *et al.*, 2018). Copper(II) complexes are redox-active and have been reported to induce oxidative stress within bacterial cells, while zinc(II) complexes, though redox-inert, exert effects by destabilizing protein and membrane structures (Kostova, 2023). Comparative investigations of identical condensation-derived ligands complexed with different metal ions remain scarce, particularly those employing standardized antibacterial assays (Szarszoń *et al.*, 2024). Direct comparative antibacterial evaluation of identical condensation-derived ligands coordinated to redox-active and redox-inert metal centers remains limited. In this study, the condensation-derived ligand 2,5,7,10-tetraaza-1,6(1,3)-dibenzenacyclodecaphene-3,4,8,9-tetraone (TF) and its complexes were synthesized and evaluated for antibacterial activity against *S. aureus* and *P. aeruginosa* to

Access this article online

https://doi.org/10.25271/sjuoz.2026.14.2.1846

Printed ISSN 2663-628X;
Electronic ISSN 2663-6298

Science Journal of University of Zakho
Vol. 14, No. 02, pp. 343 –350 April-2026

comparatively assess the influence of metal coordination on biological performance.

2. MATERIAL AND METHODS

Materials :

All chemicals used in this study were of analytical grade and procured from BDH and Fluka. FTIR spectra were recorded using a Shimadzu FTIR spectrophotometer over the range of 400–4000 cm^{-1}. Elemental (CHN) analyses were conducted on a EuroVector EA 3000 analyzer, while metal contents were determined using a PerkinElmer UN-SP9 instrument. Molar conductance measurements were performed with a Gondo PI-700PC conductivity meter (Taiwan). UV–Vis spectra were obtained using a Shimadzu UV-1900 spectrophotometer. Proton (^1H) and carbon (^{13}C) NMR spectra were recorded for the free ligand TF to confirm its structural integrity. Microwave-assisted synthesis was performed using a MO-R EM 820 oven. *Staphylococcus aureus* (ATCC 25923) and *Pseudomonas aeruginosa* (ATCC 27853) strains were obtained from the Microbiology Laboratory, Hawler Medical University, and their purity was confirmed using standard staining techniques.

Synthesis of TF:

The condensation-derived ligand TF was synthesized by a microwave-assisted condensation reaction between oxalic acid and m-phenylenediamine in the presence of cerium ammonium nitrate (CAN) as a catalyst (Scheme 1). Oxalic acid (0.180 g, 0.002 mol) and m-phenylenediamine (0.216 g, 0.002 mol) were employed in an equimolar (2:2) ratio to promote intramolecular cyclization and minimize the formation of linear oligomeric by-products. The solid reaction mixture was subjected to microwave irradiation at 900 W for 60 min. After cooling to room temperature, ethyl acetate (20 mL) was added, and the mixture was stirred for 1 hour to remove residual catalyst and low-molecular-weight by-products. The resulting solid was filtered, washed successively with ethanol and n-hexane, and dried under vacuum to afford a gray crystalline product with a yield of 82.5%. The structure of the ligand is proposed based on elemental and spectroscopic analyses.

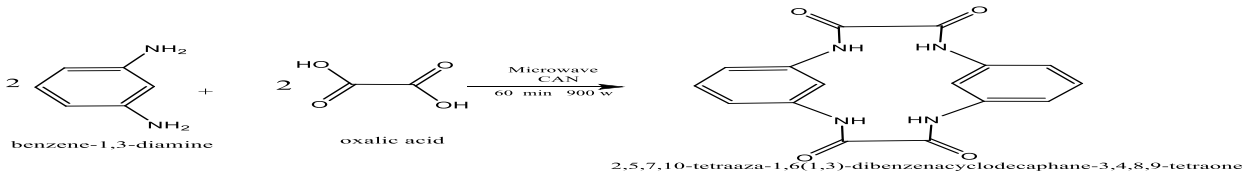

Scheme 1: Microwave-assisted cyclocondensation reaction between oxalic acid and m-phenylenediamine leading to the formation of the tetraaza ligand TF (2,5,7,10-tetraaza-1,6(1,3)-dibenzenacyclodecaphene-3,4,8,9-tetraone).

Preparation of Cu(II) and Zn(II) complexes of TF:

For complex formation, TF (0.324 g) was dissolved in a 2:2 mixture of DMF and ethanol (10 mL). To this solution, 0.001 mol of the appropriate metal salt was added: $CuCl_2 \cdot 6H_2O$ (0.237 g) for the copper complex or $ZnCl_2$ (0.139 g) for the zinc complex. The reaction mixtures were refluxed with stirring for 2 hours 15 min. The resulting precipitates were collected by filtration, washed with ethanol, and dried under vacuum to afford the metal complexes (Al-Obedi and Al-Nama, 2025; Eshankulov *et al.*, 2025; Mohammed *et al.*, 2025).

Vibrating sample magnetometer (VSM)

Figure 1 presents the vibrating sample magnetometer (VSM) curve of the Cu(II) complex [Cu(TF)], demonstrating an S-shaped hysteresis loop characteristic of paramagnetic materials. The saturation magnetization (M_s) was determined to be 3.3 emu/g, while the low values of coercivity (Hc) and remanence (Mr) are consistent with the paramagnetic behavior of the Cu(II) center (Ali *et al.*, 2024; Liu *et al.*, 2004; Maurice, 1996). Although vibrating sample magnetometry (VSM) is more commonly applied to solid-state and nanomaterials, it was employed in this study as a supplementary technique to confirm the paramagnetic behavior of the Cu(II) complex in the solid state. The obtained magnetic response is interpreted qualitatively and supports the presence of unpaired electrons consistent with Cu(II), rather than serving as a precise determination of magnetic susceptibility.

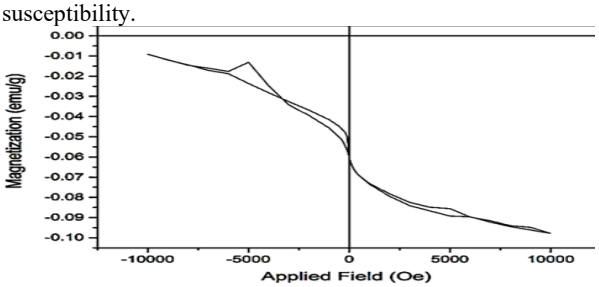

Figure 1. Vibrating sample magnetometer (VSM) hysteresis curve of the Cu(II) complex [Cu(TF)].

Electronic Spectra and Magnetic Measurements:

The UV–V is spectrum of the TF ligand reported absorption bands at 33,760 and 45,871 cm^{-1}, corresponding to n→π* and π→π* transitions, respectively. The electronic spectrum of the Cu(II) complex showed broad absorption bands in the regions 9,633–10,344 cm^{-1}, 14,679–19,047 cm^{-1}, and 23,412–32,258 cm^{-1}. These bands are attributed to spin-allowed d–d transitions of a d^9 Cu(II) ion in a distorted coordination environment. The lower-energy band in the near-infrared region can be assigned to the $^2B_1g \rightarrow {}^2A_1g$ transition, while higher-energy transitions correspond to $^2B_1g \rightarrow {}^2B_2g$ and $^2B_1g \rightarrow {}^2E$ g excitations. The considerable band broadening is consistent with Jahn–Teller distortion commonly observed in Cu(II) complexes. For the Zn(II) complex, which possesses a d^{10} electronic configuration, no d–d transitions are expected. Accordingly, the observed absorption bands are attributed exclusively to ligand-centered (π→π* and n→π*) transitions and possible ligand-to-metal charge transfer (LMCT) processes. The magnetic moment value (1.95 B.M.) lies within the expected range for mononuclear Cu(II) complexes (1.8–2.2 B.M.), indicating the presence of one unpaired electron in a d^9 configuration. The broad and asymmetric nature of the d–d absorption bands in the visible region suggests Jahn–Teller distortion, which is characteristic of octahedral or elongated square-pyramidal Cu(II) geometries. In the absence of definitive structural techniques such as single-crystal X-ray diffraction or EPR spectroscopy, the geometry is therefore best described as a distorted octahedral or pseudo-octahedral coordination environment. For the Zn(II) complex, the observed absorption bands in the UV–Vis spectrum are attributed exclusively to ligand-centered or ligand-to-metal charge transfer processes. The Zn(II) complex, possessing a d^{10} electronic configuration, is diamagnetic and exhibits only ligand-centered electronic transitions. Complexes are nonelectrolytes, according to molar conductance values, which also support an octahedral shape (Fakhree & Dawood, 2019; Jackman and Sternhell, 1969) (Tables 1 and 2). Elemental (CHN) analysis was fully performed for the free ligand TF ($C_{16}H_{12}N_4O_4$, MW = 324.30 g/mol) and showed good agreement between calculated and experimental

values, supporting its proposed structure. For the metal complexes, only metal content percentages were experimentally determined. Recalculation of theoretical metal percentages indicated that a 1:2 metal–ligand formulation would yield approximately 8% metal, which is inconsistent with the experimentally determined values (Cu: 16.56%; Zn: 16.95%). In contrast, a 1:1 metal–ligand formulation without coordinated chloride ([M(TF)]) gives theoretical metal percentages of 16.38% (Cu) and 16.78% (Zn), in excellent agreement with experimental data. Accordingly, the complexes are tentatively formulated as [M(TF)] (M = Cu, Zn). The excellent agreement between experimental and theoretical metal percentages strongly supports a 1:1 metal–ligand stoichiometry and excludes the possibility of a 1:2 formulation under the present experimental conditions. Definitive confirmation of stoichiometry and coordination environment would require complementary techniques such as mass spectrometry, EPR spectroscopy, or single-crystal X-ray diffraction.

Table 1: Physical Characteristics and Metal Analysis of TF and Its Complexes

Compound	Proposed Formula*	Color	M.P (°C)	μeff (B.M.)	Found % Metal	Theoretical % Metal	Conductance (Ω^{-1} cm^2 mol^{-1})
TF	$C_{16}H_{12}N_4O_4$	Light Brown	202–204	—	—	—	—
Cu-complex	[Cu (TF)]	Deep Brown	<400	1.95	16.56	16.38	23.4
Zn-complex	[Zn (TF)]	Pale Green	<400	Diamagnetic	16.95	16.78	20.3

*Proposed formulations are tentative and based primarily on metal percentage analysis and spectroscopic data.

Table 2: FTIR spectral assignments (cm^{-1}) and UV–Vis absorption bands of ligand TF and its Cu(II) and Zn(II) complexes.

No.	I.R.					UV-Vis.
	υ) N-H)	δ) N-H)	υ) C=O	υ(N–benzene)	υ(M-N)	λ_{max} (cm^{-1})
TF	3442	1340	1741	1546	——	33760, 45871
1	3124(w)	1262(m)	1740(m)	1437	495(m)	10344, 19047, 32258
2	3267(w)	1280(w)	1738(m)	1454	433(w)	30121, 41025

Preparation of Bacterial Suspensions:

Staphylococcus aureus (ATCC 25923) and *Pseudomonas aeruginosa* (ATCC 27853) were used as test organisms. A 24-hour culture was grown in nutrient broth at 37 °C. Bacterial cells were harvested and suspended in sterile normal saline to achieve a turbidity of 10^8–10^9 CFU/mL. Viable counts were determined using the surface drop method on nutrient agar. Serial dilutions were prepared, and 0.1ml aliquots were plated and incubated at 37 °C for 24 hours. Colony counts were used to confirm inoculum concentration. Fresh bacterial suspensions were prepared for each experiment. Dilutions corresponding to 10^{-5}–10^{-7} were used for viable count determination

Antibacterial Activity Evaluation:

Agar Well Diffusion Assay:

The antibacterial activity of the synthesized complexes, i.e., [Cu(TF)] and [Zn(TF)], was determined using the standard agar well diffusion technique. Overnight cultures of *Staphylococcus aureus* (ATCC 25923) and *Pseudomonas aeruginosa* (ATCC 27853), illustrated in **Figure 2,** were adjusted to a turbidity equivalent to a 0.5 McFarland standard. Mueller–Hinton agar plates were uniformly inoculated by lawn culture with 100 µL of the standardized bacterial suspension. Wells (6 mm in diameter) were aseptically punched into the agar and filled with 100 µL of each test complex solution at a final concentration of 1 mg/mL. Plates were aerobically incubated at 37 °C for 24 hours. The inhibition zones were then read in millimeters with a digital caliper after incubation. Each experiment was repeated at least three times, and data are the means ± SD. To enable comparative evaluation, the relative activity of the Cu(II) complex over the Zn(II) analogue was expressed as percentage increase in inhibition zone diameter. OD_{600} measurements were employed as a complementary quantitative approach to assess bacterial growth suppression in liquid culture and were not intended as a direct quantitative comparison with agar diffusion inhibition zones. Ciprofloxacin was used as a positive control, while solvent blanks were included as negative controls. The free ligand TF was evaluated under identical experimental conditions

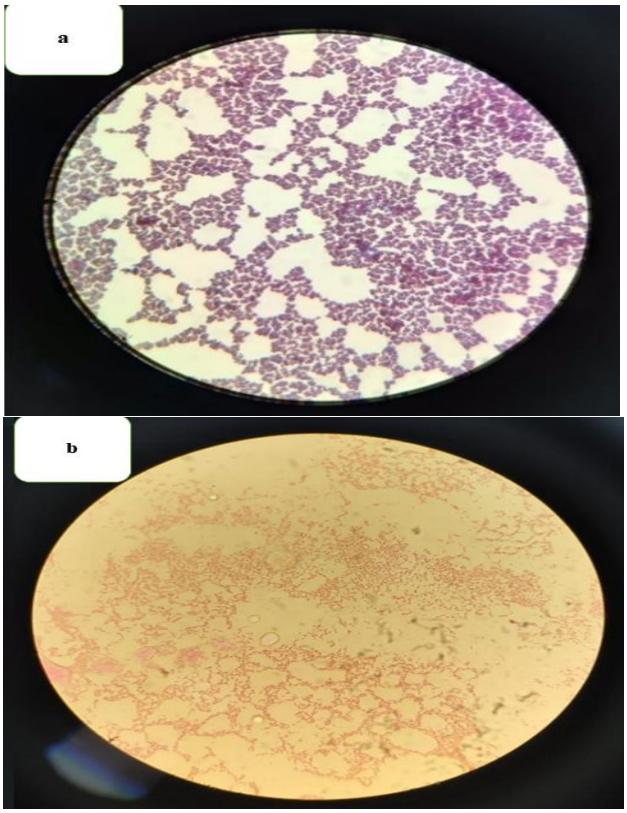

Figure 2: Morphological appearance of the tested bacterial strains: (**a**) *Staphylococcus aureus* (ATCC 25923) and (**b**)

Pseudomonas aeruginosa (ATCC 27853) used in antibacterial screening.

Statistical analysis:

The experimental data were subjected to statistical analyses using IBM SPSS Statistics, version 27.0. Results were expressed as the mean ± SD of three measurements (n = 3). Normality and homogeneity were verified prior to one-way ANOVA and Tukey's HSD post hoc comparisons ($p < 0.05$). The practical significance of pairwise comparisons was also computed using Cohen's d and interpreted according to the established criteria (small, medium, large). For the inhibition zone measurements, independent samples *t*-tests were used to compare the mean zones of B2 ([Cu (TF)]) and B3 ([Zn (TF)]) for each bacterial species. The percent relative increase of B2 over B3 was calculated to highlight the enhancement in antibacterial activity. Additionally, inhibition efficiency (IE%) and reduction factor (RF) were computed for each treatment relative to the control to quantitatively describe bacterial growth suppression. All statistical tests were two-tailed, and a p-value less than 0.05 was considered statistically significant. Statistical analysis confirmed that the inhibition zones produced by the Cu(II) complex were significantly larger than those of the Zn(II) complex and the free ligand ($p < 0.05$). Although the number of replicates was limited (n = 3), this sample size is consistent with preliminary antimicrobial screening studies, and effect size analysis (Cohen's d) was therefore emphasized to support biological relevance.

3. RESULTS AND DISCUSSIONS

The synthesized ligand TF was obtained as a gray crystalline solid with a melting point of 202–204 °C, indicating good purity and thermal stability. The key physical characteristics of the synthesized ligand TF, including appearance, melting point, solubility behavior, and isolated yield, are summarized in Table 3. The compound demonstrated good solubility in polar aprotic solvents such as DMF and DMSO, which facilitated subsequent metal complexation. The microwave-assisted condensation reaction afforded an isolated yield of 82.5%, indicating efficient cyclization under the applied reaction conditions. The structural features of TF were investigated using FTIR and NMR spectroscopy. The FTIR spectrum of the free ligand (Table 4) showed a broad band at 3442 cm^{-1} attributable to ν(N–H) stretching vibrations, a band at 1340 cm^{-1} corresponding to δ(N–H) bending, and a strong absorption at 1741 cm^{-1} assigned to ν(C=O) stretching of the amide carbonyl groups. Additional bands associated with ν(N–benzene) and amide (–CONH–CO–) functionalities further supported successful condensation between oxalic acid and m-phenylenediamine, as illustrated in Scheme 1. The ^{1}H NMR spectrum of TF (Table 5 and Figure 3) shows a characteristic singlet at δ 8.96 ppm assigned to the amide NH protons, indicating successful formation of the condensation product. The absence of free primary amine signals in the region δ 4–5 ppm, together with the presence of a distinct singlet at δ 8.96 ppm corresponding to amide NH protons, confirms successful condensation between oxalic acid and m-phenylenediamine.

Table 3: Physical Characteristics of the Synthesized Ligand (TF)

Property	Observed Value
Appearance	Gray crystalline
Melting Point (°C)	202–204
Solubility	Soluble in DMF, DMSO
Yield (%)	82.5
FTIR (key peaks, cm^{-1})	3442, 1741, 1546

Table 4: ^{1}H NMR chemical shift assignments of ligand TF in DMSO-d_6

δ (ppm)	Multiplicity	Integration	Assignment
8.96	S	2H	NH (amide)
7.9	M	2H	Ar–H
7.6	M	4H	Ar–H
7.4	m	2H	Ar–H

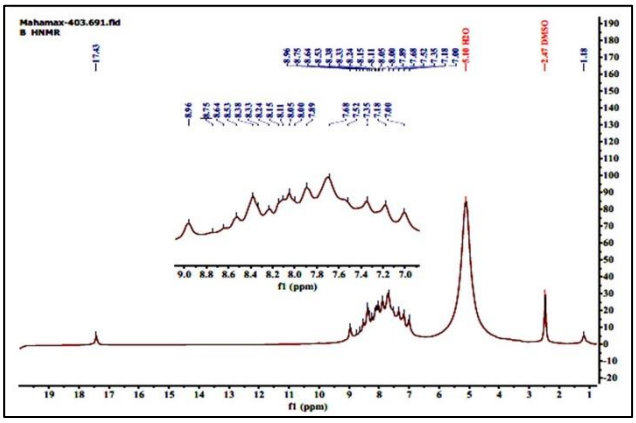

Figure 3: ^{1}H NMR spectrum of ligand TF recorded in DMSO-d_6

The aromatic proton multiplets observed between δ 7.40–7.90 ppm further supports the formation of the expected aromatic framework. In the ^{13}C NMR spectrum (Table 5 and Figure 4), the resonance at δ 160.1 ppm is consistent with amide carbonyl carbons, confirming formation of the –NH–CO–CO–NH– functionality. These data support ligand formation; however, macrocyclic ring closure cannot be conclusively established without molecular ion confirmation by ESI-MS or crystallographic analysis. Aromatic protons appear as multiplets in the region δ 7.40–7.90 ppm. The ^{13}C NMR spectrum (Table 4) revealed a strong resonance at δ 160.1 ppm corresponding to the amide carbonyl carbons, together with signals at δ 130 ppm from aromatic carbons. These data support the presence of the expected functional groups and confirm ligand formation, although they do not provide definitive proof of macrocyclic closure in the absence of mass spectrometric or crystallographic evidence. The solvent signal of DMSO-d_6 was observed at approximately 40 ppm. Collectively, these spectroscopic data confirm the presence of the expected functional groups and are consistent with the formation of a condensation-derived ligand. However, they do not provide definitive proof of a macrocyclic architecture, and the proposed structure should therefore be regarded as tentative in the absence of single-crystal X-ray diffraction or mass spectrometric confirmation. Similar spectroscopic features have been reported for structurally related condensation-derived ligands with biological relevance (Alfonso-Herrera *et al.*, 2022).

Table 5: ^{13}C NMR chemical shift assignments of ligand TF in DMSO-d_6

δ (ppm)	Assignment
160.1	C=O (amide carbonyl)
130	Aromatic carbons
55	C–N (nitrogen-bound carbon)

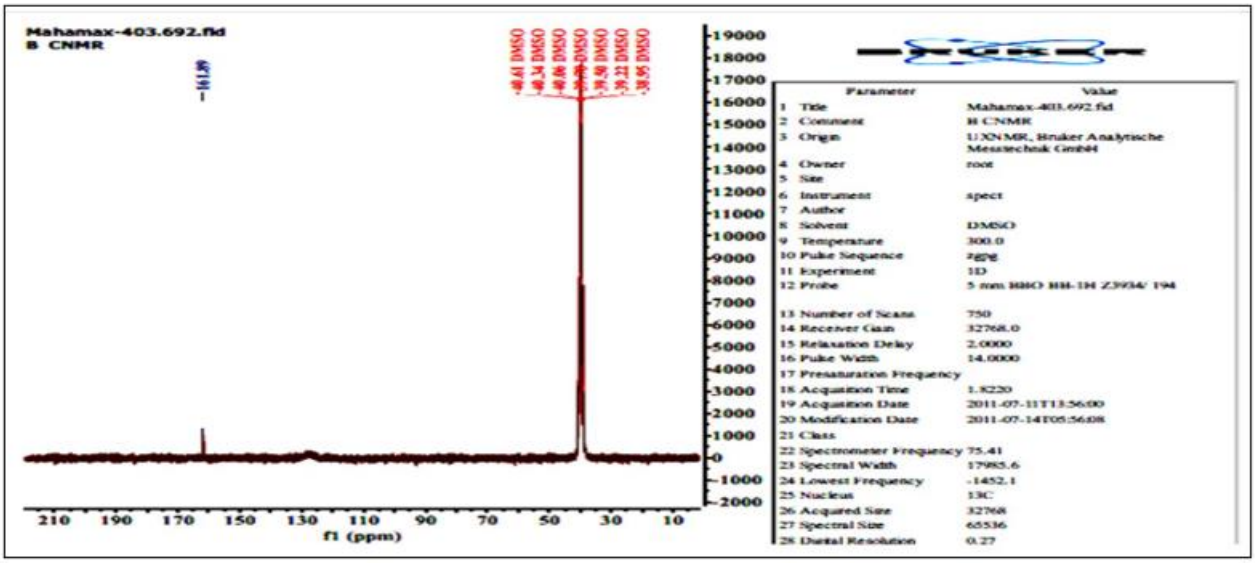

Figure 4: ^{13}C NMR spectrum of ligand TF recorded in DMSO-d_6.

The [Cu(TF)] complex was further characterized by VSM analysis. The magnetization curve displayed an S-shaped hysteresis loop with a saturation magnetization (Ms) of 3.3 emu/g, together with low coercivity (Hc) and remanence (Mr) values. These results confirmed the paramagnetic nature of the Cu(II) center and are consistent with the distorted octahedral geometry inferred from spectroscopic data. The antibacterial activity of the metal complexes, [Cu(TF)] and [Zn(TF)], was evaluated against *Staphylococcus aureus* and *Pseudomonas aeruginosa* using the agar well diffusion method. The Cu(II) complex demonstrated significantly larger inhibition zones than both the Zn(II) analogue and the free ligand, with mean inhibition zone diameters of 19 mm against S. aureus and 18 mm against *P. aeruginosa*, compared with 9 mm and 8 mm, respectively, for the Zn(II) complex (Table 6, Figures 5 and 6), compared with the Zn(II) complex (9 and 8 mm, respectively). The observed inhibition zone of 19 mm against *S. aureus* for [Cu(TF)] is comparable to the 17–22 mm range reported for structurally related Cu(II)–Schiff base complexes (El-Shafiy *et al.*, 2017, Nazirkar *et al.*, 2019). However, it remains lower than the 25–30 mm inhibition zones reported for certain highly lipophilic Cu(II) complexes containing extended conjugated systems, which have been associated with enhanced membrane permeability and stronger antibacterial potency. These comparisons indicate that the present complex exhibits competitive, though not exceptional, antibacterial activity relative of related coordination compounds. The enhanced antibacterial activity of the Cu(II) complex is consistent with its redox-active nature, which may facilitate ROS generation and membrane disruption (Mañozca-Dosman *et al.*, 2025, Sinicropi *et al.*, 2022). Weaker inhibition (<10 mm) by Zn(II) complexes, in contrast, supports redox activity as a principal mediator of antibacterial efficacy. The comparatively lower antibacterial activity of the free ligand TF may be attributed to reduced lipophilicity and limited bacterial membrane penetration in the absence of metal coordination. Statistical analysis further substantiated the observed antibacterial trends. One-way ANOVA revealed significant differences among treatments ($p < 0.05$), and post-hoc comparisons confirmed that the inhibition zones produced by the Cu(II) complex were significantly larger than those of the Zn(II) complex and the free ligand. The calculated Cohen's d values indicated large effect sizes, demonstrating that the enhanced antibacterial activity of the Cu(II) complex is not only statistically significant but also biologically meaningful.

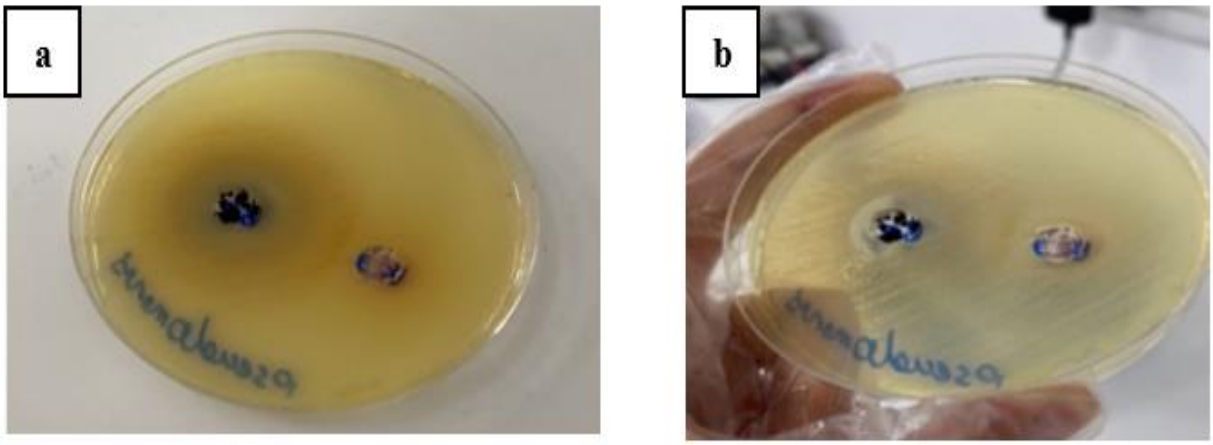

Figure 5: Agar well diffusion inhibition zones produced by (**a**) [Cu(TF)] and (**b**) [Zn(TF)] against *Pseudomonas aeruginosa* (ATCC 27853) at 1 mg/mL

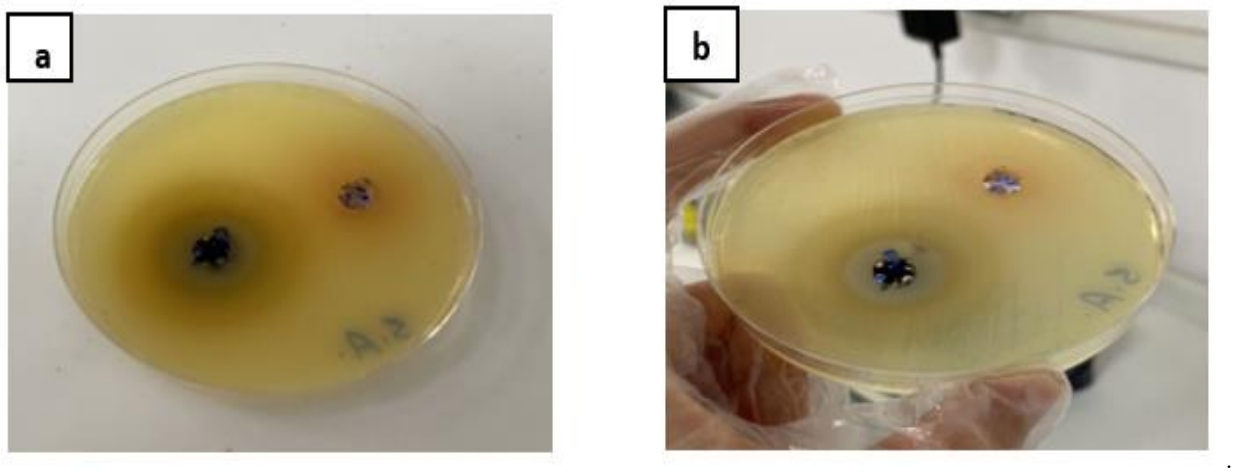

Figure 6: Agar well diffusion inhibition zones produced by (**a**) [Cu(TF)] and (**b**) [Zn(TF)] against *Staphylococcus aureus* (ATCC 25923) at 1 mg/mL.

Table 6: Mean inhibition zone diameters (mm) of [Cu(TF)] and [Zn(TF)] against *S. aureus* and *P. aeruginosa* determined by agar well diffusion assay (1 mg/mL, n = 3).

Complex	Code	*S. aureus*	*P. aeruginosa*
[Cu (TF)]	B2	19 mm	18 mm
[Zn (TF)]	B3	9 mm	8 mm

Values represent mean inhibition zone diameters (n = 3). Differences between complexes were statistically significant (one-way ANOVA followed by Tukey's HSD, $p < 0.05$). Effect size analysis indicated large practical significance (Cohen's $d > 0.8$). Differences between the inhibition zones produced by the Cu(II) and Zn(II) complexes were statistically significant for both Staphylococcus aureus and Pseudomonas aeruginosa (one-way ANOVA followed by Tukey's HSD, $p < 0.05$). Effect size analysis indicated a large practical significance (Cohen's $d > 0.8$), confirming the superior antibacterial performance of the Cu(II) complex. The inhibition of bacterial growth was evaluated with OD_{600} after treatment. High OD values (0.95 for S. aureus and 0.91 for *P. aeruginosa*) were observed in the untreated control groups, indicating significant bacterial growth of bacteria in those samples. By comparison, treatment with the Cu (II) complex caused a noticeable inhibition of growth, with OD_{600} readings of 0.22 and 0.24, respectively. The Zn(II) complex exhibited intermediate effects ($OD_{600} = 0.63$ and 0.67) (Table 7). All groups reported coefficients of variation (CV%) below 5%, demonstrating the precision and reproducibility of measurements. The OD_{600} results qualitatively supported the antibacterial trends observed in the agar diffusion assay and reflected growth inhibition under liquid culture conditions. Because agar diffusion and OD_{600} assays probe distinct biological endpoints, no direct statistical correlation between inhibition zone diameters and optical density values was attempted.

Table 7: Optical density (OD_{600}) descriptive statistics and coefficient of variation (n = 3) for bacterial growth inhibition assays.

Group	Mean OD_{600}	SD	CV%
Control *(S. aureus)*	0.95	0.03	3.16%
[Cu (TF)] (*S. aureus*)	0.22	0.01	4.55%
[Zn (TF)] (*S. aureus*)	0.63	0.02	3.17%
Control *(P. aeruginosa)*	0.91	0.04	4.40%
[Cu (TF)] *(P. aeruginosa)*	0.24	0.01	4.17%
[Zn (TF)] *(P. aeruginosa)*	0.67	0.02	2.99%

Despite the promising antibacterial activity observed, the present study has important limitations related to structural confirmation and mechanistic interpretation. The proposed coordination modes and molecular formulations are primarily based on spectroscopic and elemental metal content analyses and would benefit from further confirmation using advanced structural techniques, such as mass spectrometry, EPR spectroscopy (for Cu(II)), and single-crystal X-ray diffraction. Additionally, mechanistic insights into antibacterial activity, including reactive oxygen species generation, membrane disruption, and molecular target interactions, were not directly investigated. Future studies incorporating these analyses, together with in vivo toxicity and efficacy evaluations, will be essential to fully establish the therapeutic potential of these metal-based antimicrobial agents.

CONCLUSION

In the present study, a condensation-derived ligand (TF) and its corresponding Cu(II) and Zn(II) coordination complexes were successfully synthesized and comparatively evaluated using complementary spectroscopic and biological assays. FTIR and UV–Vis spectral analyses provide supportive evidence for coordination of the ligand to the metal centers primarily through nitrogen donor atoms, while the carbonyl groups remain non-coordinating. Elemental metal percentage analysis supports a 1:1 metal–ligand stoichiometry for both complexes, which are tentatively formulated as [M(TF)] (M = Cu, Zn). The Cu(II) complex revealed paramagnetic behavior consistent with a distorted octahedral geometry, whereas the Zn(II) complex is diamagnetic, in agreement with its d^{10} electronic configuration.

Antibacterial evaluation against *Staphylococcus aureus* and *Pseudomonas aeruginosa* demonstrated that metal coordination significantly influences biological activity, with the Cu(II) complex showing markedly higher antibacterial efficacy than both the Zn(II) complex and the free ligand. This enhancement is plausibly associated with the redox-active nature of Cu(II), which may facilitate oxidative stress and disruption of bacterial cellular processes. Although enhanced antibacterial activity was observed upon metal coordination, the present study should be regarded as a preliminary comparative assessment rather than a definitive structure activity relationship investigation. Despite the promising antibacterial performance observed for the Cu(II) complex, the present investigation remains a preliminary coordination and screening study. The absence of definitive structural elucidation techniques, such as EPR spectroscopy or single-crystal X-ray diffraction, limits the precision with which structure activity relationships can be established. Future investigations should integrate advanced structural, mechanistic, and cytotoxicity evaluations to fully assess therapeutic relevance. The limited number of complexes and the absence of definitive structural elucidation preclude rigorous correlation between molecular structure and biological response. Although mass spectrometric (ESI-MS) confirmation was not available at the time of this study due to instrumental limitations, the combined evidence from metal percentage analysis, spectroscopic data, magnetic measurements, and molar conductance strongly supports the proposed formulation. Future studies will incorporate ESI-MS and single-crystal X-ray diffraction to provide definitive structural confirmation.

Acknowledgments:

The authors would like to thank Hawler Medical University for providing laboratory facilities and support for this study.

Author Contributions:

F.M.D.: Conceptualization, methodology, formal analysis, supervision. M.Q.Q.: Writing – original draft preparation, data curation, investigation. S.S.A.: Methodology, validation, laboratory work, data analysis. L.A.A.: Data interpretation, writing, review, and editing. T.Y.Y.: Statistical analysis, validation, data visualization. R.R.K.: Supervision, project administration, writing, review and editing, corresponding author.

Conflict of Interest:

The authors declare that there are no conflicts of interest regarding the publication of this paper.

Ethical Statement:

This study was reviewed and approved by the Medical Ethics Committee of Hawler Medical University, Erbil, Iraq, under approval code F/08/2025. This study did not involve human participants or clinical samples. All experimental procedures were conducted in accordance with institutional guidelines and ethical standards.

REFERENCES

Al-Obedi, A. D., & Al-Nama, K. S. (2025). Computational binding studies and bioactivity evaluation for certain Schiff base metal-complexes transformed from ciprofloxacin. Kimya Problemleri, 23(3), 449–461. https://doi.org/10.32737/32221-38688-2025-32733-32449-32461

Alfonso-Herrera, L. A., Rosete-Luna, S., Hernández-Romero, D., Rivera-Villanueva, J. M., Olivares-Romero, J. L., Cruz-Navarro, J. A., *et al*. (2022). Transition metal complexes with tridentate Schiff bases (ONO and ONN) derived from salicylaldehyde: An analysis of their potential anticancer activity. ChemMedChem, 17(20), e202200367. https://doi.org/10.1002/cmdc.202200367

Ali, E. M., Iqbal, A., Ibrahim, M. N. M., Alheety, M. A., Ahmed, N. M., Yanto, D. H. Y., *et al*. (2024). Magnetic attapulgite synthesized via sonochemistry: An innovative strategy for efficient solid-phase extraction of As^{3+} from simulated and unrefined crude oil samples. Journal of Porous Materials, 31(4), 1183–1195. https://doi.org/10.1007/s10934-024-01581-9

Almatroudi, A. (2025). Biofilm resilience: Molecular mechanisms driving antibiotic resistance in clinical contexts. Biology, 14(2), 165. https://doi.org/10.3390/biology14020165

Claudel, M., Schwarte, J. V., & Fromm, K. M. (2020). New antimicrobial strategies based on metal complexes. Chemistry, 2(4), 849–899. https://doi.org/10.3390/chemistry2040056

El-Lateef, H. M. A., El-Dabea, T., Khalaf, M. M., & Abu-Dief, A. M. (2023). Recent overview of potent antioxidant activity of coordination compounds. Antioxidants, 12(2), 213. https://doi.org/10.3390/antiox12020213

El-Shafiy, H. F., Saif, M., Mashaly, M. M., Halim, S. A., Eid, M. F., Nabeel, A., *et al*. (2017). New nano-complexes of Zn(II), Cu(II), Ni(II) and Co(II) ions: Spectroscopy, thermal, structural analysis, DFT calculations and antimicrobial activity application. Journal of Molecular Structure, 1147, 452–461. https://doi.org/10.1016/j.molstruc.2017.06.112

Eshankulov, K. N., Turaev, K. K., Geldiev, Y., Nomozov, A., Eshankulov, S., Musaev, C. A., *et al.* (2025). Studying of metal-containing acrylic copolymers and sulfur-modified bitumen BH 90/30. Kimya Problemleri, 23(2), 202–213. https://doi.org/10.32737/32221-38688-2025-32732-32202-32213

Fakhree, M., & Dawood, S. K. (2019). Preparation and characterization of some transition metal complexes with two mixed ligands macrocyclic and PPh_3 ligands. Rafidain Journal of Science, 28(5), 29–37. https://doi.org/10.33899/rjs.2019.163294

Jackman, L. M., & Sternhell, S. (1969). Applications of nuclear magnetic resonance in organic chemistry (2nd ed.). Pergamon Press.

Khan, E., Hanif, M., & Akhtar, M. S. (2022). Schiff bases and their metal complexes with biologically compatible metal ions: Biological importance, recent trends and future hopes. Reviews in Inorganic Chemistry, 42(4), 307–325. https://doi.org/10.1515/revic-2021-0034

Kollef, M. H., Torres, A., Shorr, A. F., Martin-Loeches, I., & Micek, S. T. (2021). Nosocomial infection. Critical Care Medicine, 49(2), 169–187. https://doi.org/10.1097/CCM.0000000000004783

Kostova, I. (2023). The role of complexes of biogenic metals in living organisms. Inorganics, 11(2), 56. https://doi.org/10.3390/inorganics11020056

Liu, X., Ma, Z., Xing, J., & Liu, H. (2004). Preparation and characterization of amino-silane modified superparamagnetic silica nanospheres. Journal of Magnetism and Magnetic Materials, 270(1–2), 1–6. https://doi.org/10.1016/j.jmmm.2003.07.006

Mañozca-Dosman, I. V., Aragón-Muriel, A., & Polo-Cerón, D. (2025). Antibacterial activity of metal complexes of Cu(II) and Ni(II) with the ligand 2-(phenylsubstituted) benzimidazole. Scientia Pharmaceutica, 93(2), 22. https://doi.org/10.3390/scipharm93020022

Maurice, P. A. (1996). Applications of atomic-force microscopy in environmental colloid and surface chemistry. Colloids and Surfaces A: Physicochemical and Engineering

Aspects, 107, 57–75. https://doi.org/10.1016/0927-7757(95)03372-6

Mohammed, E. H., AlSultan, M., Alasalli, S. M., & Sabah, A. A. (2025). Syntheses, characterization and thermal stability study of new Co(II), Cu(II) and Zn(II) complexes derived from Schiff base 4-(dimethylamino)benzaldehyde. Kimya Problemleri, 23(3), 395–406. https://doi.org/10.32737/32221-38688-2025-32733-32395-32406

Muteeb, G., Rehman, M. T., Shahwan, M., & Aatif, M. (2023). Origin of antibiotics and antibiotic resistance, and their impacts on drug development: A narrative review. Pharmaceuticals, 16(11), 1615. https://doi.org/10.3390/ph16111615

Nazirkar, B., Mandewale, M., & Yamgar, R. (2019). Synthesis, characterization and antibacterial activity of Cu(II) and Zn(II) complexes of 5-aminobenzofuran-2-carboxylate Schiff base ligands. Journal of Taibah University for Science, 13(1), 440–449. https://doi.org/10.1080/16583655.2019.1592316

Riccardi, L., Genna, V., & De Vivo, M. (2018). Metal–ligand interactions in drug design. Nature Reviews Chemistry, 2(7), 100–112. https://doi.org/10.1038/s41570-018-0018-6

Salam, M. A., Al-Amin, M. Y., Salam, M. T., Pawar, J. S., Akhter, N., Rabaan, A. A., *et al*. (2023). Antimicrobial resistance: A growing serious threat for global public health. Healthcare, 11, 1947. https://doi.org/10.3390/healthcare11131947

Sinicropi, M. S., Ceramella, J., Iacopetta, D., Catalano, A., Mariconda, A., Rosano, C., *et al*. (2022). Metal complexes with Schiff bases: Data collection and recent studies on biological activities. International Journal of Molecular Sciences, 23(23), 14840. https://doi.org/10.3390/ijms232314840

Szarszoń, K., Andrä, S., Janek, T., & Wą tły, J. (2024). Insights into the chemistry, structure, and biological activity of human salivary MUC7 fragments and their Cu(II) and Zn(II) complexes. Inorganic Chemistry, 63(25), 11616–11627. https://doi.org/10.1021/acs.inorgchem.4c00868